

Personalized Generative Low-light Image Denoising and Enhancement

Xijun Wang, Prateek Chennuri, Yu Yuan, Bole Ma, Xingguang Zhang, Stanley Chan
Purdue University

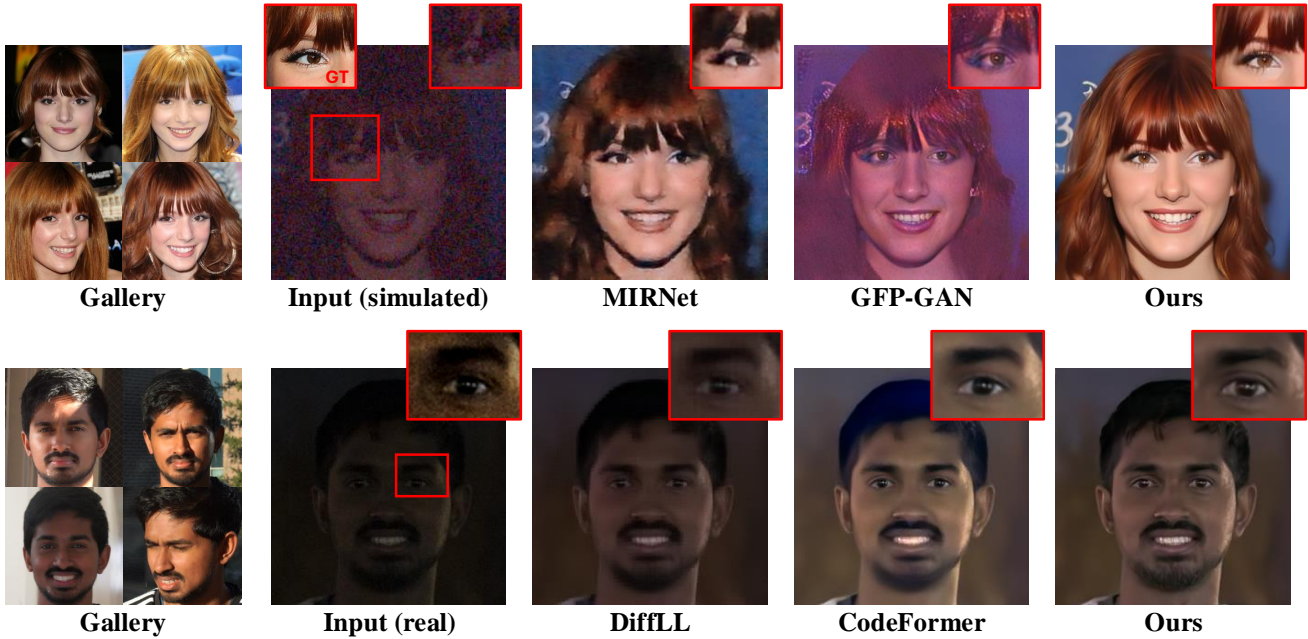


Figure 1. Using gallery from a phone user, we can restore low-light noisy facial images. Our method produces finer details and better identity consistency compared to other state-of-the-art restoration approaches like MIRNet [61, 62], GFP-GAN [52], DiffLL [22] and CodeFormer [67] on both simulated (top row) and real-captured (bottom row) low-light noisy inputs.

Abstract

Modern cameras produce remarkably high-quality images, yet their performance in low-light conditions remains sub-optimal due to fundamental limitations in photon shot noise and sensor read noise. While generative image restoration methods have shown promising results compared to traditional approaches, they often suffer from hallucinatory content generation when the signal-to-noise ratio (SNR) is low. Leveraging the availability of personalized photo galleries on users’ smartphones, we introduce Diffusion-based Personalized Generative Denoising (DiffPGD), a novel approach that builds a customized diffusion model for individual users. Our key innovation lies in the development of an identity-consistent physical buffer that extracts the physical attributes of the person from the gallery. This ID-

consistent physical buffer serves as a robust prior that can be seamlessly integrated into the diffusion model to restore degraded images without the need for fine-tuning. Over a wide range of low-light testing scenarios, we show that DiffPGD achieves superior image denoising and enhancement performance compared to existing diffusion-based denoising approaches.

1. Introduction

With the astonishing development of smartphones, it is safe to say that smartphone cameras today have surpassed digital single-lens reflex (DSLR) cameras in both popularity and functionality. However, the small form factor of smartphone cameras puts a tight constraint on the aperture size, hence limiting the amount of light a CMOS pixel can detect. In a low-light imaging environment, this creates a fundamental limitation to how short the minimum exposure needs to be

[†]Project page: <https://genai-restore.github.io/DiffPGD/>.

and how much signal-to-noise ratio (SNR) the sensor can support. While some of the noise seen at low light can be mitigated using better CMOS technology (e.g., correlated double sampling to reduce the read noise [41] and deep-well pump gate to reduce the stray capacitance between the floating diffusion and the transfer gate [39, 40]), the Poisson / Bose-Einstein statistics due to random photon arrivals is a problem created by mother nature that cannot be solved by even the ideal sensors. Therefore, image denoising and enhancement by exploiting the internal structures of images become a necessary task for all smartphone cameras.

From a signal-processing perspective, degradation caused by low light can be roughly approximated via

$$\mathbf{y} = \text{ADC}(\text{Poisson}(\alpha\mathbf{x} + \eta)) + \epsilon, \quad (1)$$

where \mathbf{x} is the unknown clean image, α is the sensor gain, η is the dark current, and ϵ is the read noise. The inverse problem associated with low-light denoising is to recover \mathbf{x} from \mathbf{y} . Over the past five decades, the main driving force is to exploit image structures, from Wiener filter [36], total variation [4, 44], wavelets [9] to non-local means [3], BM3D [10], and recently convolution neural networks [2, 6, 18, 25, 50, 57, 64], transformers [35, 38, 63], and diffusion models [26, 60, 68]. A common theme across existing methods is to find and utilize a *generic* prior $p(\mathbf{x})$, i.e., a prior learned from a large collection of example images. While they perform well in moderately difficult problems, the generality of these methods cannot be extended to heavily corrupted images. Particularly in the context of human face recovery, the restored results often lack real identity and exhibit artifacts. This is attributed to the ill-posed nature of the problem and the lack of appropriate constraints.

Why Gallery Photos? Smartphone cameras today typically store hundreds if not thousands of a user’s photos, captured at different times, in different places, and under different lighting conditions. While these images have many variations, they are all about the same person(s). Therefore, if the imaging goal is to take a photo of this user, the gallery on the phone would be the best source to build a prior $p(\mathbf{x})$. This concept is illustrated in Fig. 2. In the context of diffusion-based image restoration, the initial solution space can be large since many candidate solutions are consistent with the noisy observation. The gallery provides a strong constraint to the search problem. This allows us to search for better quality images and preserve the person’s identity.

There are, however, two technical questions:

- What class of images we should focus on: In this paper, we focus on *human faces* because of their relevance to phone users. We assume that the gallery photos have

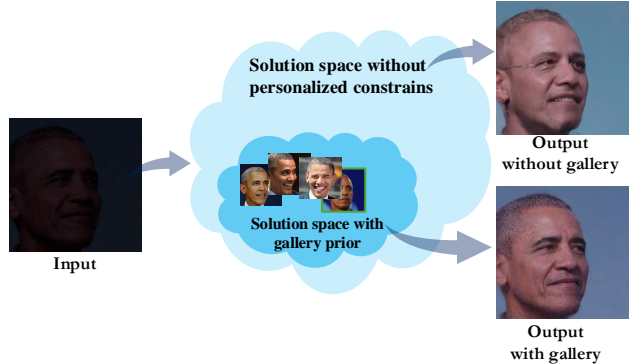


Figure 2. The restoration of inputs degraded by noise and low-light conditions is highly ill-posed. By incorporating additional high-quality gallery photos of the same identity, we significantly reduce the solution space, thereby achieving improved identity consistency in the restored images.

been selected and are reasonably informative. Product-level engineering such as pre-processing and selection of the gallery photos is important but beyond the scope of this paper.

- How to incorporate the class-specific $p(\mathbf{x})$ into the restoration model: The bigger (and harder) question is that given the gallery photos, how do we efficiently extract the prior information and improve the restoration? We do not want to train a restoration model from the scratch because the gallery can be small. We want to avoid fine-tuning as much as possible during inference. Moreover, the person’s identity needs to be preserved.

Physical Buffers to the Rescue. Given the gallery photos, what kind of prior information would be useful for restoration? Advancements in computer vision have made it possible to extract facial *physical buffers*—including albedo and normal maps—from a person’s gallery of images [43, 47, 65]. These physical buffers capture crucial identity-defining properties such as surface geometry and skin color, effectively encoding an individual’s unique identity. At the same time, it also eliminates the external influence of environmental lighting, pose, and other identity-independent variables. By incorporating this robust prior that disentangles the external influences, our approach can effectively extract identity information from the gallery.

Contributions. Our contributions are threefold:

1. **Personalized Low-Light Denoise and Enhancement Framework:** We introduce a new framework that leverages diffusion models and person-specific priors from photo galleries to denoise low-light facial images while preserving the identity.
2. **Physical Identity Buffers:** We propose the use of physical identity buffers from existing face galleries to enrich

the restoration process, enabling accurate reconstruction of human faces under severe degradation.

3. **Easy Deployment:** Our method operates easily without requiring fine-tuning for individual users, making it practical and scalable to multiple users.

Extensive experiments demonstrate that our approach outperforms existing techniques in both visual quality and identity preservation, providing a significant advancement in low-light facial image restoration.

2. Related Works

Low-light Image Enhancement and Denoising. Low-light images often suffer from significant noise due to low signal-to-noise ratios (SNR), in addition to reduced brightness and contrast. Traditional low-light denoising techniques often focus on exploiting image structures, ranging from early methods like Wiener filtering [36], total variation [4, 44], and wavelets [9] to non-local means [3] and BM3D [10]. More recently, deep learning approaches, including convolutional neural networks [2, 6, 18, 25, 50, 57, 64, 66], transformers [35, 38, 63], and diffusion-based models [26, 42, 60, 68], have emerged as promising solutions for low-light denoising. Low-light image enhancement (LLIE) aims to improve the brightness and contrast of images captured in poorly lit conditions. Traditional approaches [16, 29, 31] often leverage heuristic or physical models to enhance image quality, while learning-based methods [5, 17, 22, 24, 28, 37, 53, 56, 59] have demonstrated greater effectiveness when supported by large-scale datasets. Recent advancements [38, 42, 45, 58] in this field have increasingly focused on jointly addressing denoising and enhancement tasks, aiming to improve image quality while effectively suppressing noise to maintain natural appearance. However, to the best of our knowledge, no specific approach currently exists for joint enhancement and denoising of facial images in low-light conditions.

Deep Face Restoration. CNN/Transformer-based face restoration methods [14, 23, 54], such as RestoreFormer [54], typically rely on paired low- and high-quality image datasets to learn resolution enhancement and noise reduction. While effective, these methods often struggle under severe degradation and lack the capability to synthesize realistic details in complex scenarios.

In recent years, generative priors have been increasingly utilized in face restoration to better address real-world degradations. GAN-based methods, such as GFP-GAN [52], leverage StyleGAN2 [49] to enhance facial details, while diffusion-based models [7, 13, 48, 51, 55] have further expanded restoration capabilities. For instance, BFRDiffusion [7] uses Stable Diffusion to enhance low-quality images by adding high-fidelity details, and Ding *et al.* [13]

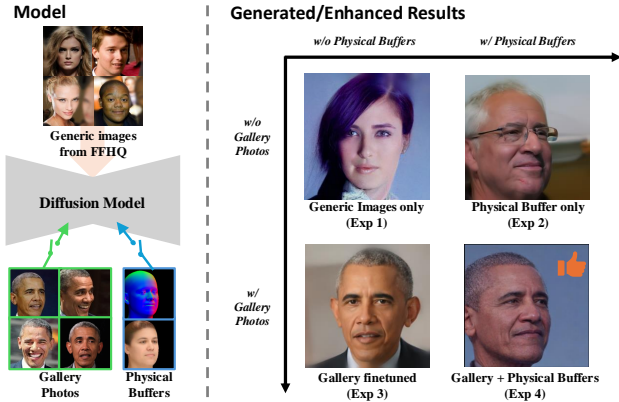


Figure 3. Path to the idea. Using facial physical buffers and gallery images can help preserve human face identity information.

employ a pretrained diffusion model that denoises degraded inputs while preserving identity by fine-tuning on a person’s gallery photos. MGBFR [48] combines text prompts and reference images with a dual-control adapter to retain accurate facial attributes and identity. Although these generative methods are effective, they often rely on multi-stage training or finetuning, which can limit the efficient use in some real-world applications.

Reference Prior for Face Restoration. In face restoration, reference images [13, 32, 33, 48] provide essential priors for recovering detailed and high-frequency facial features. These priors guide the model to generate realistic restorations. Reference-based methods can be divided into two types: single reference and gallery-based images. The single reference approach [48] uses one image to guide the restoration, focusing on enhancing facial details from a specific reference. In contrast, the gallery-based approach [13] leverages multiple reference images, offering more diverse information and stronger constraints, improving the accuracy and realism of the restoration. Despite the effectiveness [13] using gallery photos of users, it still requires multi-stage training and fine-tuning on each user during inference.

3. Method

3.1. Restoration by Diffusion

A diffusion model approximates the clean image distribution $p_\theta(\mathbf{x}_0)$ by learning a model θ that reverses the noise-adding process. In Denoising Diffusion Probabilistic Models (DDPMs) [21], Gaussian noise is progressively added to a clean image \mathbf{x}_0 :

$$\mathbf{x}_t = \sqrt{\alpha_t}\mathbf{x}_0 + \sqrt{1 - \alpha_t}\epsilon, \quad \text{where } \epsilon \sim \mathcal{N}(\mathbf{0}, \mathbf{I}). \quad (2)$$

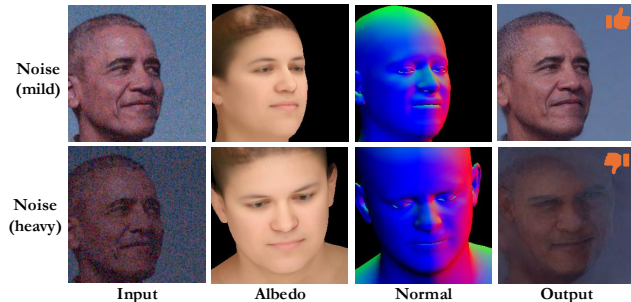


Figure 4. For images affected by mild low-light noise, physical buffers can be accurately extracted. However, when encountering the images degraded by severe low light and noise, precise physical buffers are difficult to obtain.

The reverse process then removes the noise to reconstruct the clean image. After training, for any given time t and the corresponding noisy image \mathbf{x}_t , the model can iteratively denoise by sampling from $p(\mathbf{x}_0|\mathbf{x}_t)$.

In restoration tasks, like low-light denoising, the goal is to recover a high-quality image \mathbf{x}_0 from a low-quality input \mathbf{y} . Unlike pure generation, where the output can be any image that follows the distribution of clean images, restoration is constrained by the content of \mathbf{y} . During training, the model uses \mathbf{y} as a condition, and once the model is trained, for any given time t and the corresponding noisy image \mathbf{x}_t , it can iteratively denoise by sampling from $p(\mathbf{x}_0|\mathbf{x}_t, \mathbf{y})$ using the trained model.

3.2. Why Combining Gallery and Physical Buffer?

We formalize our core approach of extracting identity-consistent physical buffers from gallery photos to guide the diffusion model for restoration. This method is based on the observation that using facial physical buffers or gallery images can help preserve identity information during restoration tasks involving diffusion models. To evaluate the capability of physical buffers and gallery images, we conducted four simple experiments under a blind scheme (excluding y_0 during training), as illustrated in Fig. 3:

- **Exp 1:** Model trained solely on generic images (purely generative).
- **Exp 2:** Model trained on generic images, conditioned on the facial physical buffer extracted from the input image.
- **Exp 3:** Model trained on generic images, then fine-tuned with the user’s gallery photos.
- **Exp 4:** Model trained on generic images, fine-tuned with the user’s gallery photos, and conditioned on the facial physical buffer.

We tested these models on a mildly noisy input. Exp 1 produces random faces, as expected from a purely generative model. In contrast, Exp 2 uses physical buffers obtained via

DECA [15], which can extract coarse face buffers from a single 2D photo (see Fig. 4), yielding faces with user-like features (e.g., nose shape, mouth and skin tone). Hence, physical buffers can convey key identity cues. Exp 3 outputs distinct faces of the same user, compared to Exp1, showing that fine-tuning with gallery photos effectively transfers identity information. Finally, Exp 4 yields the best results, showcasing that the collaborative use of gallery photos and facial physical prior can achieve the optimal outcomes.

While Fig. 3 shows us a design direction, we need to overcome:

- Fine-tuning:** Extracting identity via fine-tuning requires significant time and must be repeated for each user. Additionally, the small size of a gallery compared with a large pre-trained model can lead to overfitting.
- Unreliable buffers from degraded inputs:** As studied in the face reconstruction literature, low-quality inputs consistently present additional challenges [15]. Severe degradation undermines the extraction of physical buffers (Fig. 4), resulting in poor reconstruction. Moreover, features captured from a single degraded photo are limited, not to mention from a degraded one.

In conclusion, to avoid repeated fine-tuning on galleries and reduce the risk of erroneous buffers from noisy inputs, it is more desirable to jointly employ gallery photos and facial physical priors, as we will discuss below.

3.3. Extracting Physical Buffer from Photo Gallery

Based on the preceding analysis, we propose extracting physical buffers directly from existing clean gallery photos and using them as conditions to guide the diffusion model during training. This approach offers significant benefits: clean gallery photos allow us to form comprehensive and robust identity-consistent physical buffers containing more accurate facial identity features of the target person. Specifically, We will extract the albedo and normal maps of the target person, which are two key attributes used to describe the physical characteristics of a face.

- **Albedo** captures the intrinsic color of an object’s surface—that is, the subject’s color properties without any lighting effects. It reveals a person’s facial appearance, e.g. eyebrows, lip coloration, and other distinct texture elements can reflect individual identity traits.
- **Normal** encodes the surface orientation at each pixel, which provides hints about the underlying shape characteristics.

By conditioning on these identity physical buffers, we eliminate the need to fine-tune the model with gallery images and avoid the issue of incorrect buffer extraction. Consequently, the model is better equipped to preserve the target person’s identity and facial features, even under severe

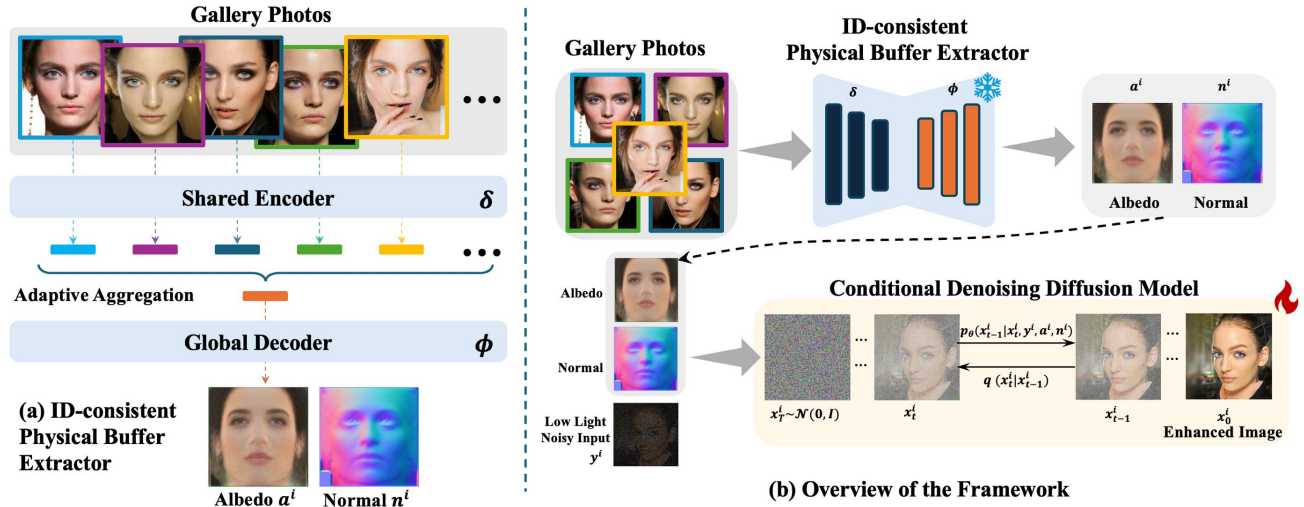


Figure 5. The overall architecture of the proposed method. Our core idea is to use ID-consistent physical buffers, extracted from gallery photos, to constrain the generative space in the diffusion model restoration process. For a high-quality gallery, we use LAP [65] to extract the albedo and normal information for each photo and apply adaptive aggregation to fuse the entire gallery. The extracted albedo represents base skin color and facial appearance, while normal captures facial geometry. In our framework, the output physical buffers isolate the intrinsic ID properties from lighting, shading, and pose, enabling the diffusion model to apply only ID-related information consistently.

degradation.

However, extracting physical buffers for a person from a set of gallery photos is a more challenging task than extracting these buffers from a single input, as in methods like DECA. This complexity arises because gallery photos of the same person are often taken under varying conditions, such as different scenes and poses. To ensure these buffers comprehensively represent the person’s identity and facial properties, they must be aligned to maintain identity consistency. As shown in the physical buffer extractor module in Fig. 5(a), we adopt the aggregation net design from the LAP [65] to extract the *ID-consistent* physical buffers, which adaptively combines facial features from multiple images to learn consistent geometry and texture representations, and generates ID-consistent albedo and normal maps from a photo collection of the same individual.

3.4. Model Framework

We name our final proposed model **DiffPGD**. As illustrated in Fig. 5, the model leverages ID physical buffers (albedo a^i and normal n^i) extracted from person i ’s gallery photos as conditions to guide our diffusion model during training directs the generative process toward a personalized space.

The aggregation network contains a shared encoder δ across multiple images and a global decoder ϕ for predicting the consistent representation. To model albedo and normal, two separate aggregation networks, denoted as (δ^a, ϕ^a) and

(δ^n, ϕ^n) , are employed. Given a photo gallery of N images $\{\mathbf{F}_k^i\}_{k=1}^N$ of person i , each image is processed by δ^a and δ^n to extract its texture and geometry latent codes α_k^a and α_k^n , respectively. To derive a global representation of the identity for person i based on $\{\alpha_k^a, \alpha_k^n\}_{k=1}^N$, an adaptive aggregation method is adopted. This method learns a weight set $\{\mathbf{w}_k^a, \mathbf{w}_k^n\}_{k=1}^N$ according to the quality of each image in $\{\mathbf{F}_k^i\}_{k=1}^N$. The combined global ID-code α_c^a and α_c^n for texture and depth are calculated as:

$$\alpha_c^a = \sum_{k=1}^N \mathbf{w}_k^a \alpha_k^a, \text{ and } \alpha_c^n = \sum_{k=1}^N \mathbf{w}_k^n \alpha_k^n. \quad (3)$$

Once calculated, the global ID-code α_c^a and α_c^n are passed to the decoders ϕ^a and ϕ^n , respectively, to produce the ID-consistent albedo \mathbf{a}^i and normal \mathbf{n}^i .

During inference, the process begins with a Gaussian noise image \mathbf{x}_T^i , which is iteratively transformed into the clean, enhanced image \mathbf{x}_0^i by sampling from $p(\mathbf{x}_0^i | \mathbf{x}_T^i, \mathbf{y}^i, \mathbf{a}^i, \mathbf{n}^i)$ using the trained model. With the low-light noisy image \mathbf{y}^i as another condition during training, other features, such as pose, hairstyle, and background inside the image beyond facial features can be effectively captured as well.

Our experiments demonstrate that identity information is effectively preserved with the guidance of these ID-consistent buffers, enabling our model to achieve superior results in human face restoration.

4. Experiments

4.1. Dataset

Training Data. Since no publicly available datasets exist for low-light noisy face images, we simulate such data using the CelebAMask-HQ dataset [30], the InverseISP algorithm [34], and the Poisson-Gaussian noise model Eq. (1). The pipeline involves converting RGB images to their corresponding RAW mosaiced format using InverseISP [34], followed by applying Eq. (1) to simulate low-light noise using realistic camera sensor parameters. Multiple noise levels are generated by varying the light intensity (Lux) to ensure the model is robust across diverse noise conditions. *Refer to supplementary for more details on the simulation.*

Testing Data. For testing DiffPGD, we utilize both simulated and real-world captured low-light noisy data.

The simulation setup assumes a 12-bit image sensor with parameters similar to that of Canon DSLR cameras: a Full Well Capacity of $36000e^-$, Quantum Efficiency of 0.42, dark current of $7e^-$, and read noise of $6e^-$. These parameters ensure realistic noise characteristics for evaluating model performance.

We also captured 100 RAW-format face images as real-world test dataset using a Sony $\alpha 6400$ DSLR camera paired with a Sony 18-135mm lens at night. These images feature diverse low-light and dark backgrounds, various angles and poses, as well as different focal lengths, apertures, ISO values, and shutter speeds to reflect the rich characteristics of real-world low-light photography. We cropped these images into 256×256 face patches.

4.2. Implementation Details

Our denoising model is built on the ADM architecture [12], and the ID-consistent physical extractor is implemented using the aggregation network from LAP [65]. For training, we use a P2-weighted loss function [8], which measures the discrepancy between the predicted and ground-truth noise. This loss is defined as: $L = \lambda_t \|\hat{\epsilon}_t - \epsilon_t\|_2^2$, where λ_t serves as a hyperparameter to adjust the loss weight dynamically across different timesteps.

During the training stage, we train our model on the CelebAMask-HQ dataset [30], comprising 30,000 images distributed across 4,516 unique identities (IDs). We use 3318 IDs for training and 200 IDs for simulated testing. Within each ID, there are 3–20 images. The number of gallery images we used per person varies from 3 to 6, with most around 5. The Adam optimizer is applied with a learning rate of $1e-4$. Training is performed for 200,000 iterations with a batch size of 32, resulting in a total of 6,400,000 samples seen by the model.

4.3. Performance in Real-Captured Scenarios

Testing model performance in real-life low-light scenarios is crucial and challenging, as real-world conditions often involve uncontrollable factors compared to simulated ones. Since no existing data set addresses the restoration of real-life low-light noisy face photos, we captured photos of real persons under indoor and outdoor low-light scenarios, as illustrated in Section 4.1.

We compare our methods with several state-of-the-art works: UTV-Net[66], GFPGAN[52], SNR-aware[59], MIRNet[61, 62], DiffLL[22], Codeformer [67]. These works aim to restore high-quality images from degraded data that has been affected by low light, noise, or both, which are close to the subject of our research. Particularly, GFPGAN and Codeformer are designed specifically for face image restoration, which is highly competitive with our method. We re-trained/fine-tuned all the baselines with the same training dataset as ours for fair comparison.

Quantitative and qualitative results are presented. To assess the quality of restored images, we employ the Fréchet Inception Distance (FID) [20] and the Kernel Inception Distance (KID) [1], as these metrics offer a robust evaluation aligned with human perception. Since ground-truth images are unavailable for real-captured cases, we compute the FID and KID score between the model’s output and the corresponding subjects’ gallery photos. As shown in Fig. 6, our method produces images with the highest quality and level of detail. The restored images exhibit more natural skin tones and well-preserved facial identity features, such as eye shape, eyebrows, and lips, while maintaining the highest consistency in facial identity.

Since our work focuses on face images, we also check on the identity preservation performance. Besides the image quality metrics, we adopt the identity score which calculates the cosine similarity of the image features extracted by ArcFace[11] to further evaluate the identity consistency. Again, since ground truth images are unavailable for real-captured cases, we calculate the identity (ID) score by averaging the ID scores between the model’s output images and each gallery photo of the corresponding subjects. The results are also shown in Table 2. Again, our method has the highest identity score, and the visual results are consistent with the quantitative metric results. The results demonstrate the supreme ability of our proposed DiffPGD model on real low light denoising and enhancement task.

4.4. Performance in Simulated Scenarios

In simulated scenarios, We use the 200 test images which correspond to the 200 test IDs from CelebAMask-HQ and send them into our simulator to generate the test set. We simulated various low-light noisy levels by setting different

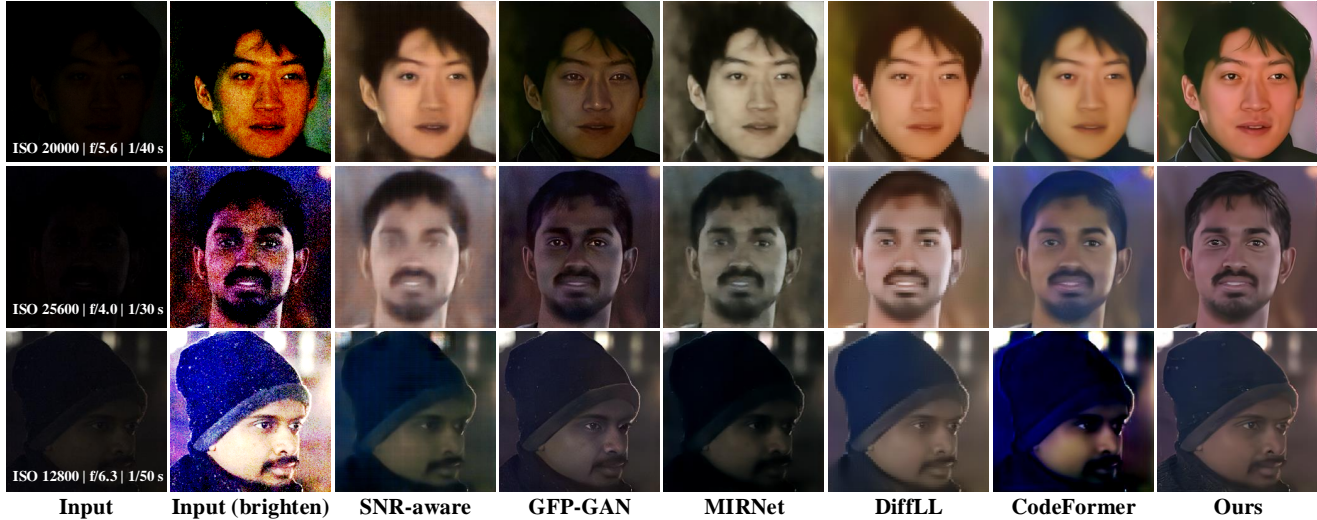


Figure 6. Visual comparison on real cases. The first column presents the input images along with their capture parameters. In the second column, we enhance the brightness to better reveal the noise. Please zoom in for the best visual experience.

Photons Per Pixel	5				10				13				26			
	ID Score \uparrow	FID \downarrow	KID \downarrow	PSNR \uparrow	ID Score \uparrow	FID \downarrow	KID \downarrow	PSNR \uparrow	ID Score \uparrow	FID \downarrow	KID \downarrow	PSNR \uparrow	ID Score \uparrow	FID \downarrow	KID \downarrow	PSNR \uparrow
SNR-aware[59]	0.2156	188.3311	0.1302	8.4541	0.4240	139.8193	0.0786	9.5462	0.4999	124.1162	0.0626	10.1712	0.6937	99.9875	0.0383	12.4961
MIRNet[61, 62]	0.1229	294.7381	0.2414	8.6008	0.2860	214.7785	0.1534	9.8572	0.3830	187.2571	0.1286	10.4209	0.6212	136.1320	0.0793	12.8992
DiffLL[22]	0.2910	167.3905	0.1068	17.3506	0.4544	150.4559	0.1117	18.3360	0.5095	140.2738	0.0996	19.9547	0.6833	119.2693	0.0760	23.3180
GFPGAN[52]	0.1941	388.9293	0.4256	7.1990	0.2075	233.3173	0.1521	8.1283	0.2976	190.7264	0.1326	9.5483	0.5976	158.9475	0.0829	11.4855
CodeFormer[67]	0.2863	111.4544	0.04908	18.2406	0.4940	91.1244	0.0326	19.2692	0.5563	84.7955	0.0281	20.2306	0.7338	80.6582	0.0263	24.5512
Ours	0.3714	77.5743	0.0084	17.9334	0.5225	71.8645	0.0063	18.4999	0.5938	69.5567	0.0042	19.0910	0.7118	59.1975	0.0030	23.7226

Table 1. Quantitative comparison with state-of-the-art works on CelebAMask-HQ dataset on 5PPP, 10PPP, 13PPP, and 26PPP. The lower the PPP, severe the degradation is.

photons per pixel (PPP), i.e., the average number of photons arriving at the sensor within the exposure time. The lower the PPP, severe the degradation is. A lower photon level increases the impact of read noise and dark current on the final output, thereby decreasing the quality of the reconstructed images.

Quantitative results are provided in Table 1. The image restored from our method has the highest quality and more details, meanwhile preserving the facial identity and maintaining the ID consistent best. (Refer to supplementary for more visual comparisons). From the table, we could see that CodeFormer surpasses us on PSNR. Fig. 7 illustrates a visual comparison between our method and CodeFormer under inputs ranging from 5 to 65 PPP. We observe that CodeFormer tends to generate smoother images while we could preserve better high-frequency details. Furthermore, our method demonstrates superior identity preservation even at low resolutions, such as 5 PPP to 13 PPP, while exhibiting fewer artifacts. The advantage of our model in maintaining identity consistency is particularly evident in heavily degraded cases. The results highlight the strong performance of our proposed DiffPGD model in low-light denoising and

enhancement tasks.

Methods	FID \downarrow	KID \downarrow	ID Score \uparrow
SNR-aware[55]	252.2397	0.1264	0.1990
UTVNet[66]	341.8502	0.1617	0.2002
MIRNet[61, 62]	276.3853	0.1659	0.2210
DiffLL[22]	252.1553	0.1421	0.3196
GFPGAN[52]	252.7411	0.1249	0.1525
CodeFormer[67]	281.9744	0.1459	0.2965
Ours	251.9318	0.0882	0.3708

Table 2. Comparisons with state-of-the-art works on the real-captured test cases.

Methods	FID \downarrow	KID \downarrow	ID Score \uparrow
w/o physical buffers	272.6148	0.1281	0.3169
w/ physical buffers	251.9318	0.0882	0.3708

Table 3. Ablation comparisons of using ID physical buffers on real-captured photo test.

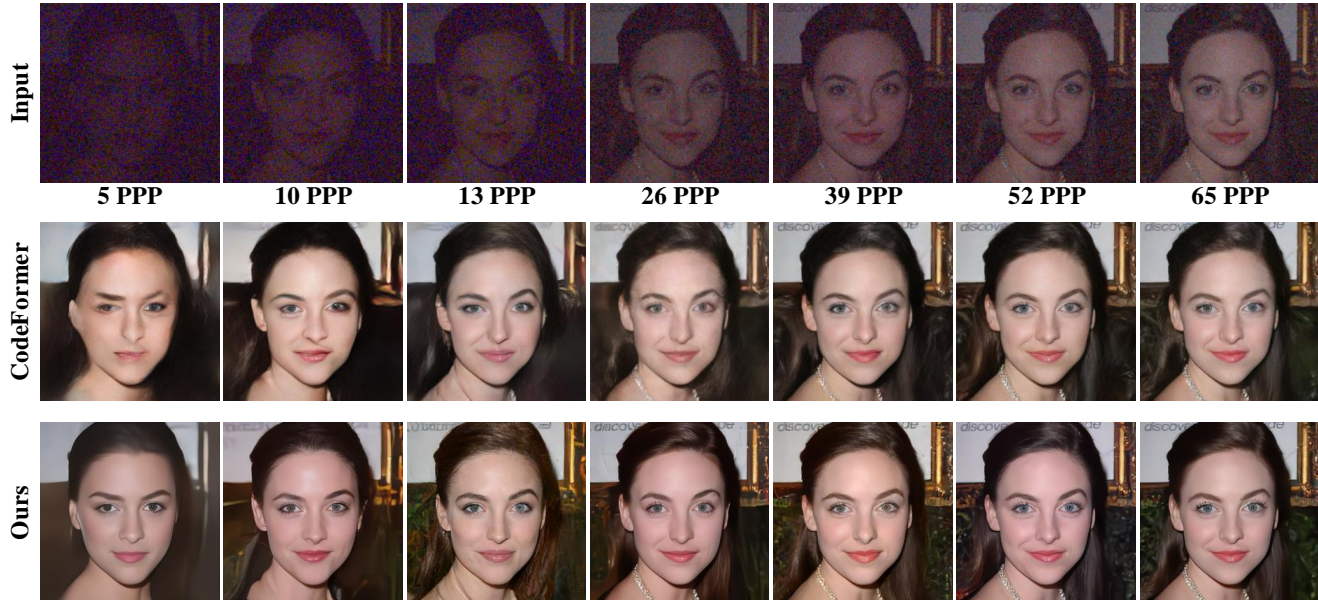


Figure 7. Visual comparison on the simulated cases. Our method maintains good identity consistency even at extremely low PPP and exhibits fewer artifacts.

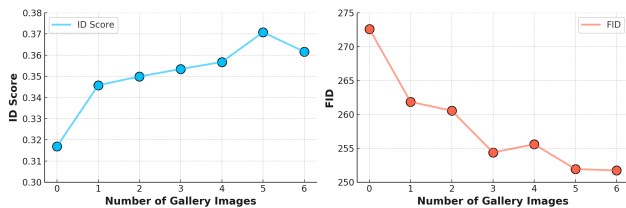


Figure 8. The relationship between the identity (ID) score and FID of the restored images and the number of gallery images used to generate the ID physical buffer.

5. Ablation Study

ID-Consistent Physical Buffers for Identity Preservation. We have shown that the proposed model DiffPGD exhibits outstanding performance in both simulated and real-captured testing scenarios. In Table 3, we compare the quantitative results of training our model with and without ID physical buffers in real-captured test cases. The results demonstrate that using physical buffers largely increases the identity score, highlighting the effectiveness of extracting ID physical buffers from a person’s existing photo gallery to assist in restoring real-world low-quality photos.

Effect of the Number of Gallery Images. The proposed DiffPGD model is conditioned with the ID physical buffers extracted from the User’s gallery photos. As claimed in the paper, facial features extracted from a single image are inherently limited. In Fig. 8, we evaluate the effect of the number of gallery images used to generate the ID physi-

cal buffer. We analyze it with the real-captured set where 6 gallery images were collected from each subject. The results show that identity preservation improves as the ID physical buffer is derived from a greater number of gallery photos rather than a single image. Additionally, incorporating the ID physical buffer significantly enhances identity preservation compared to not using it, which corresponds to the case without gallery photos.

6. Conclusion

In this work, we addressed the challenges of low-light facial image restoration by introducing Diffusion-based Personalized Generative Denoising (DiffPGD), a novel approach that leverages user-specific photo galleries to improve denoising performance. By incorporating an identity-consistent physical buffer, we provided a strong prior that enhances the diffusion model’s ability to restore degraded images while avoiding the need for model fine-tuning. Our experiments, which included extensive evaluations on multiple challenging datasets, demonstrated that DiffPGD not only outperforms existing diffusion-based denoising methods but also delivers superior quantitative and qualitative results across various testing scenarios. This approach effectively mitigates false content generation in low-SNR conditions while bridging the gap in low-light imaging quality, ultimately paving the way for personalized and more robust image restoration techniques.

References

- [1] Mikołaj Bińkowski, Dougal J. Sutherland, Michael Arbel, and Arthur Gretton. Demystifying mmd GANs. In *International Conference on Learning Representations*, 2018. 6
- [2] Tim Brooks, Ben Mildenhall, Tianfan Xue, Jiawen Chen, Dillon Sharlet, and Jonathan T. Barron. Unprocessing images for learned raw denoising. In *IEEE/CVF Conference on Computer Vision and Pattern Recognition (CVPR)*, pages 11028–11037, 2019. 2, 3
- [3] A. Buades, B. Coll, and J.-M. Morel. A non-local algorithm for image denoising. In *IEEE Conference on Computer Vision and Pattern Recognition (CVPR)*, pages 60–65, 2005. 2, 3
- [4] A Chambolle. An algorithm for total variation minimization and applications. *Journal of Mathematical Imaging and Vision*, 20:89–97, 2004. 2, 3
- [5] Chen Chen, Qifeng Chen, Jia Xu, and Vladlen Koltun. Learning to see in the dark. In *IEEE/CVF Conference on Computer Vision and Pattern Recognition (CVPR)*, pages 3291–3300, 2018. 3
- [6] Jingwen Chen, Jiawei Chen, Hongyang Chao, and Ming Yang. Image blind denoising with generative adversarial network based noise modeling. In *IEEE/CVF Conference on Computer Vision and Pattern Recognition (CVPR)*, pages 3155–3164, 2018. 2, 3
- [7] Xiaoxu Chen, Jingfan Tan, Tao Wang, Kaihao Zhang, Wenhan Luo, and Xiaochun Cao. Toward real-world blind face restoration with generative diffusion prior. *IEEE Transactions on Circuits and Systems for Video Technology*, 34(9): 8494–8508, 2024. 3
- [8] Jooyoung Choi, Jungbeom Lee, Chaehun Shin, Sungwon Kim, Hyunwoo Kim, and Sungroh Yoon. Perception prioritized training of diffusion models. In *IEEE/CVF Conference on Computer Vision and Pattern Recognition (CVPR)*, pages 11472–11481, 2022. 6
- [9] R. R. Coifman and D. L. Donoho. *Translation-Invariant Denoising*, pages 125–150. 1995. 2, 3
- [10] Kostadin Dabov, Alessandro Foi, Vladimir Katkovnik, and Karen Egiazarian. Image denoising by sparse 3-d transform-domain collaborative filtering. *IEEE Transactions on Image Processing*, 16(8):2080–2095, 2007. 2, 3
- [11] Jiankang Deng, Jia Guo, Niannan Xue, and Stefanos Zafeiriou. Arcface: Additive angular margin loss for deep face recognition. In *IEEE/CVF conference on computer vision and pattern recognition (CVPR)*, pages 4690–4699, 2019. 6
- [12] Prafulla Dhariwal and Alexander Nichol. Diffusion models beat gans on image synthesis. *Advances in neural information processing systems*, 34:8780–8794, 2021. 6, 13
- [13] Zheng Ding, Xuaner Zhang, Zhuowen Tu, and Zhihao Xia. Restoration by generation with constrained priors. In *IEEE/CVF Conference on Computer Vision and Pattern Recognition (CVPR)*, 2024. 3
- [14] Yingruo Fan, Zhaojiang Lin, Jun Saito, Wenping Wang, and Taku Komura. FaceFormer: Speech-driven 3d facial animation with transformers. In *IEEE/CVF Conference on Computer Vision and Pattern Recognition (CVPR)*, 2022. 3
- [15] Yao Feng, Haiwen Feng, Michael J Black, and Timo Bolkart. Learning an animatable detailed 3d face model from in-the-wild images. *ACM Transactions on Graphics*, 40(4):1–13, 2021. 4
- [16] Xueyang Fu, Delu Zeng, Yue Huang, Xiao-Ping Zhang, and Xinghao Ding. A weighted variational model for simultaneous reflectance and illumination estimation. In *IEEE/CVF Conference on Computer Vision and Pattern Recognition (CVPR)*, pages 2782–2790, 2016. 3
- [17] Chunle Guo, Chongyi Li, Jichang Guo, Chen Change Loy, Junhui Hou, Sam Kwong, and Runmin Cong. Zero-reference deep curve estimation for low-light image enhancement. In *IEEE/CVF Conference on Computer Vision and Pattern Recognition (CVPR)*, pages 1777–1786, 2020. 3
- [18] Shi Guo, Zifei Yan, Kai Zhang, Wangmeng Zuo, and Lei Zhang. Toward convolutional blind denoising of real photographs. In *IEEE/CVF Conference on Computer Vision and Pattern Recognition (CVPR)*, pages 1712–1722, 2019. 2, 3
- [19] Kaiming He, Xiangyu Zhang, Shaoqing Ren, and Jian Sun. Deep residual learning for image recognition. In *IEEE/CVF conference on computer vision and pattern recognition (CVPR)*, pages 770–778, 2016. 13
- [20] Martin Heusel, Hubert Ramsauer, Thomas Unterthiner, Bernhard Nessler, and Sepp Hochreiter. GANs trained by a two time-scale update rule converge to a local nash equilibrium. In *Advances in Neural Information Processing Systems*, 2017. 6
- [21] Jonathan Ho, Ajay Jain, and Pieter Abbeel. Denoising diffusion probabilistic models. In *Advances in Neural Information Processing Systems*, page 6840–6851, 2020. 3
- [22] Hai Jiang, Ao Luo, Haoqiang Fan, Songchen Han, and Shuaicheng Liu. Low-light image enhancement with wavelet-based diffusion models. *ACM Transactions on Graphics*, 42(6):1–14, 2023. 1, 3, 6, 7
- [23] Kui Jiang, Zhongyuan Wang, Peng Yi, Tao Lu, Junjun Jiang, and Zixiang Xiong. Dual-Path deep fusion network for face image hallucination. *IEEE Transactions on Neural Networks and Learning Systems*, 33(1):378–391, 2022. 3
- [24] Yifan Jiang, Xinyu Gong, Ding Liu, Yu Cheng, Chen Fang, Xiaohui Shen, Jianchao Yang, Pan Zhou, and Zhangyang Wang. EnlightenGAN: Deep light enhancement without paired supervision. *IEEE Transactions on Image Processing*, 30:2340–2349, 2021. 3
- [25] Kyong Hwan Jin, Michael T. McCann, Emmanuel Froustey, and Michael Unser. Deep convolutional neural network for inverse problems in imaging. *IEEE Transactions on Image Processing*, 26(9):4509–4522, 2017. 2, 3
- [26] Bahjat Kawar, Michael Elad, Stefano Ermon, and Jiaming Song. Denoising diffusion restoration models. In *Advances in Neural Information Processing Systems*, 2022. 2, 3
- [27] Diederik P Kingma. Adam: A method for stochastic optimization. *arXiv preprint arXiv:1412.6980*, 2014. 13
- [28] Edwin H Land and John J McCann. Lightness and retinex theory. *JOSA*, 1971. 3
- [29] Chulwoo Lee, Chul Lee, and Chang-Su Kim. Contrast enhancement based on layered difference representation of 2d histograms. *IEEE Transactions on Image Processing*, 22(12):5372–5384, 2013. 3

- [30] Cheng-Han Lee, Ziwei Liu, Lingyun Wu, and Ping Luo. MaskGAN: Towards diverse and interactive facial image manipulation. In *IEEE Conference on Computer Vision and Pattern Recognition (CVPR)*, 2020. 6, 12
- [31] Mading Li, Jiaying Liu, Wenhan Yang, Xiaoyan Sun, and Zongming Guo. Structure-revealing low-light image enhancement via robust retinex model. *IEEE Transactions on Image Processing*, 27(6):2828–2841, 2018. 3
- [32] Xiaoming Li, Wenyu Li, Dongwei Ren, Hongzhi Zhang, Meng Wang, and Wangmeng Zuo. Enhanced blind face restoration with multi-exemplar images and adaptive spatial feature fusion. In *IEEE/CVF Conference on Computer Vision and Pattern Recognition (CVPR)*, 2020. 3
- [33] Xiaoming Li, Shiguang Zhang, Shangchen Zhou, Lei Zhang, and Wangmeng Zuo. Learning dual memory dictionaries for blind face restoration. *IEEE Transactions on Pattern Analysis and Machine Intelligence*, 2022. 3
- [34] Zhihao Li, Ming Lu, Xu Zhang, Xin Feng, M Salman Asif, and Zhan Ma. Efficient visual computing with camera raw snapshots. *IEEE Transactions on Pattern Analysis and Machine Intelligence*, 2024. 6, 12
- [35] Jingyun Liang, Jiezhong Cao, Guolei Sun, Kai Zhang, Luc Van Gool, and Radu Timofte. SwinIR: Image restoration using swin transformer. In *IEEE/CVF International Conference on Computer Vision Workshops*, pages 1833–1844, 2021. 2, 3
- [36] Jae S. Lim. Two-dimensional signal and image processing. 1989. 2, 3
- [37] Kun Lu and Lihong Zhang. TBEFN: A two-branch exposure-fusion network for low-light image enhancement. *IEEE Transactions on Multimedia*, 23:4093–4105, 2021. 3
- [38] Yucheng Lu and Seung-Won Jung. Progressive joint low-light enhancement and noise removal for raw images. *IEEE Transactions on Image Processing*, 31:2390–2404, 2022. 2, 3
- [39] Jiaju Ma and Eric R. Fossum. A pump-gate jot device with high conversion gain for a quanta image sensor. *IEEE Journal of the Electron Devices Society*, 3(2):73–77, 2015. 2
- [40] Jiaju Ma, Stanley Chan, and Eric R. Fossum. Review of quanta image sensors for ultralow-light imaging. *IEEE Transactions on Electron Devices*, 69(6):2824–2839, 2022. 2
- [41] Junichi Nakamura. *Image Sensors and Signal Processing for Digital Still Cameras*. CRC Press, 2006. 2
- [42] Cindy M Nguyen, Eric R Chan, Alexander W Bergman, and Gordon Wetzstein. Diffusion in the dark: A diffusion model for low-light text recognition. In *IEEE/CVF Winter Conference on Applications of Computer Vision (CVPR)*, 2024. 3
- [43] Joseph Roth, Yiyang Tong, and Xiaoming Liu. Adaptive 3d face reconstruction from unconstrained photo collections. In *IEEE/CVF conference on computer vision and pattern recognition (CVPR)*, pages 4197–4206, 2016. 2
- [44] L.I. Rudin and S. Osher. Total variation based image restoration with free local constraints. In *International Conference on Image Processing*, pages 31–35, 1994. 2, 3
- [45] Yiqi Shi, Duo Liu, Liguang Zhang, Ye Tian, Xuezhi Xia, and Xiaojing Fu. ZERO-IG: Zero-shot illumination-guided joint denoising and adaptive enhancement for low-light images. In *IEEE/CVF Conference on Computer Vision and Pattern Recognition (CVPR)*, pages 3015–3024, 2024. 3
- [46] Jiaming Song, Chenlin Meng, and Stefano Ermon. Denoising diffusion implicit models. *arXiv preprint arXiv:2010.02502*, 2020. 13
- [47] Supasorn Suwajanakorn, Steven M Seitz, and Ira Kemelmacher-Shlizerman. What makes tom hanks look like tom hanks. In *IEEE/CVF international conference on computer vision (ICCV)*, pages 3952–3960, 2015. 2
- [48] Keda Tao, Jinjin Gu, Yulun Zhang, Xiucheng Wang, and Nan Cheng. Overcoming false illusions in real-world face restoration with multi-modal guided diffusion model. *arXiv preprint arXiv: 2410.04161*, 2024. 3
- [49] Omer Tov, Yuval Alaluf, Yotam Nitzan, Or Patashnik, and Daniel Cohen-Or. Designing an encoder for stylegan image manipulation. *ACM Trans. Graph.*, 40(4), 2021. 3
- [50] Subarna Tripathi, Zachary C. Lipton, and Truong Q. Nguyen. Correction by projection: Denoising images with generative adversarial networks, 2018. 2, 3
- [51] Tuomas Varanka, Tapani Toivonen, Soumya Tripathy, Guoying Zhao, and Erman Acar. PFStorer: Personalized face restoration and super-resolution. In *IEEE/CVF Conference on Computer Vision and Pattern Recognition (CVPR)*, pages 2372–2381, 2024. 3, 13
- [52] Xintao Wang, Yu Li, Honglun Zhang, and Ying Shan. Towards real-world blind face restoration with generative facial prior. In *IEEE/CVF conference on computer vision and pattern recognition (CVPR)*, pages 9168–9178, 2021. 1, 3, 6, 7
- [53] Yufei Wang, Yi Yu, Wenhan Yang, Lanqing Guo, Lap-Pui Chau, Alex C Kot, and Bihan Wen. Exposurediffusion: Learning to expose for low-light image enhancement. In *IEEE International Conference on Computer Vision (ICCV)*, 2023. 3
- [54] Zhouxia Wang, Jiawei Zhang, Runjian Chen, Wenping Wang, and Ping Luo. RestoreFormer: High-quality blind face restoration from undegraded key-value pairs. In *IEEE/CVF Conference on Computer Vision and Pattern Recognition (CVPR)*, pages 17491–17500, 2022. 3
- [55] Zhixin Wang, Ziyang Zhang, Xiaoyun Zhang, Huangjie Zheng, Mingyuan Zhou, Ya Zhang, and Yanfeng Wang. Dr2: Diffusion-based robust degradation remover for blind face restoration. In *IEEE/CVF Conference on Computer Vision and Pattern Recognition (CVPR)*, pages 1704–1713, 2023. 3, 7
- [56] Chen Wei, Wenjing Wang, Wenhan Yang, and Jiaying Liu. Deep retinex decomposition for low-light enhancement. In *British Machine Vision Conference*, 2018. 3
- [57] Kaixuan Wei, Ying Fu, Jiaolong Yang, and Hua Huang. A physics-based noise formation model for extreme low-light raw denoising. In *IEEE/CVF Conference on Computer Vision and Pattern Recognition (CVPR)*, 2020. 2, 3
- [58] Ke Xu, Xin Yang, Baocai Yin, and Rynson WH Lau. Learning to restore low-light images via decomposition-and-enhancement. In *IEEE/CVF conference on computer vision and pattern recognition (CVPR)*, pages 2281–2290, 2020. 3

- [59] Xiaogang Xu, Ruixing Wang, Chi-Wing Fu, and Jiaya Jia. Snr-aware low-light image enhancement. In *IEEE/CVF conference on computer vision and pattern recognition (CVPR)*, pages 17714–17724, 2022. [3](#), [6](#), [7](#)
- [60] Cheng Yang, Lijing Liang, and Zhixun Su. Real-world denoising via diffusion model, 2023. [2](#), [3](#)
- [61] Syed Waqas Zamir, Aditya Arora, Salman Khan, Munawar Hayat, Fahad Shahbaz Khan, Ming-Hsuan Yang, and Ling Shao. Learning enriched features for real image restoration and enhancement. In *European Conference on Computer Vision (ECCV)*, pages 492–511. Springer, 2020. [1](#), [6](#), [7](#)
- [62] Syed Waqas Zamir, Aditya Arora, Salman Khan, Munawar Hayat, Fahad Shahbaz Khan, Ming-Hsuan Yang, and Ling Shao. Learning enriched features for fast image restoration and enhancement. *IEEE Transactions on Pattern Analysis and Machine Intelligence*, 2022. [1](#), [6](#), [7](#)
- [63] Jiale Zhang, Yulun Zhang, Jinjin Gu, Jiahua Dong, Linghe Kong, and Xiaokang Yang. Xformer: Hybrid x-shaped transformer for image denoising. In *International Conference on Learning Representations*, 2024. [2](#), [3](#)
- [64] Kai Zhang, Wangmeng Zuo, Yunjin Chen, Deyu Meng, and Lei Zhang. Beyond a gaussian denoiser: Residual learning of deep cnn for image denoising. *IEEE Transactions on Image Processing*, 26(7):3142–3155, 2017. [2](#), [3](#)
- [65] Zhenyu Zhang, Yanhao Ge, Renwang Chen, Ying Tai, Yan Yan, Jian Yang, Chengjie Wang, Jilin Li, and Feiyue Huang. Learning to aggregate and personalize 3d face from in-the-wild photo collection. In *IEEE/CVF Conference on Computer Vision and Pattern Recognition (CVPR)*, pages 14214–14224, 2021. [2](#), [5](#), [6](#)
- [66] Chuanjun Zheng, Daming Shi, and Wentian Shi. Adaptive unfolding total variation network for low-light image enhancement. In *IEEE/CVF international conference on computer vision (ICCV)*, pages 4439–4448, 2021. [3](#), [6](#), [7](#)
- [67] Shangchen Zhou, Kelvin Chan, Chongyi Li, and Chen Change Loy. Towards robust blind face restoration with codebook lookup transformer. *Advances in Neural Information Processing Systems*, 35:30599–30611, 2022. [1](#), [6](#), [7](#)
- [68] Yuanzhi Zhu, Kai Zhang, Jingyun Liang, Jie Zhang Cao, Bihan Wen, Radu Timofte, and Luc Van Gool. Denoising diffusion models for plug-and-play image restoration. In *IEEE Conference on Computer Vision and Pattern Recognition Workshops (NTIRE)*, 2023. [2](#), [3](#)

Supplementary Material

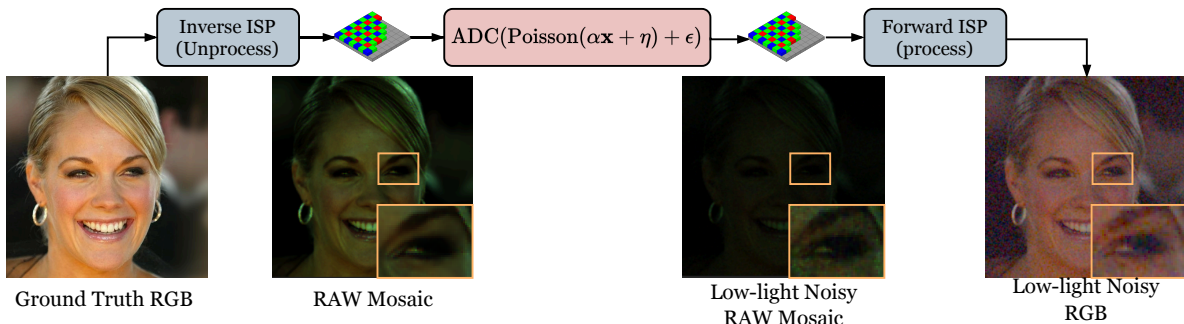


Figure 9. Simulation process for generating low-light noisy face images.

A. Dataset

As mentioned in Section 4.1 of the main paper, since no open-sourced low-light noisy datasets are available, we adopt a simulation approach to generate low-light noisy face images for training our model. Specifically, we utilize the CelebAMask-HQ dataset’s [30] face images as the ground truth RGB images.

As shown in Fig. 9, the first step in the simulation process involves passing the RGB image through a pre-trained Inverse ISP network [34] to generate a pseudo ground truth RAW mosaic image. For visualization purposes, we display the demosaiced version of this image. We utilize the pretrained weights provided by the authors [34], which were obtained by training the network on iPhone camera images, for unprocessing the RGB images into RAW format.

This pseudo ground truth RAW image is then passed through a Poisson-Gaussian Simulator to simulate the low-light noisy RAW mosaic image. It is noteworthy that during the training process, we vary the camera sensor parameters (in the Poisson-Gaussian simulator) across a wide range of values to enable the model to handle diverse camera sensor noise profiles. The simulation setup assumes a 12-bit image sensor with parameters similar to those of Canon DSLR cameras. The parameter ranges are summarized in Table 5.

Parameter	Range
Full Well Capacity	$[19000e^-, 64000e^-]$
Quantum Efficiency	$[0.32, 0.54]$
Dark Current	$[2.2e^-, 11.7e^-]$
Read Noise	$[2.2e^-, 10.8e^-]$
Photons-per-Pixel (PPP)	$[13 \text{ PPP}, 65 \text{ PPP}]$

Table 5. Simulation parameters used in the Poisson-Gaussian Simulator.

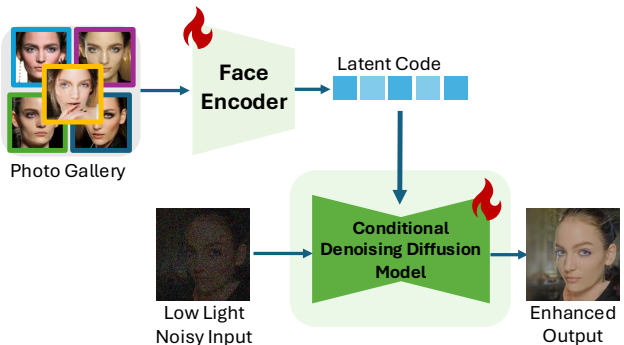


Figure 10. A network architecture diagram for identity feature restoration using a face encoder.

These parameters are carefully chosen to ensure realistic noise characteristics during training.

B. Additional Visual Results

In Fig. 12, Fig. 14, and Fig. 15, we present additional visual comparisons between our model and baseline methods on real-captured and simulated cases. Our results consistently demonstrate superior performance, particularly in cases of severe degradation.

Methods	PSNR \uparrow	SSIM \uparrow	LPIPS \downarrow	ID Score \uparrow
w/ Encoder	12.62	0.2574	0.6315	0.6906
w/ physical buffers	13.85	0.3753	0.6042	0.8039

Table 6. Comparison of ID physical buffers and encoder-based methods on the real-captured photo test set. For a fair comparison, we use two same gallery images for each individual for both the encoder-based and physical buffer-based approaches.

C. More Implementation Details

During training and testing, the image size is 256×256 . The architecture of the diffusion model is adapted from [12]. We modify the architecture so that the model can take the concatenation of physical buffers and degraded images as conditions. The model parameters are configured as follows: the number of channels is set to 128, channel multiple is (1, 1, 2, 2, 4, 4), head channels are 128, attention resolution is 16, dropout rate is 0.1, diffusion steps are 1000, and the two hyperparameters $P2_gamma$ and $p2_k$ are both set to 1.0. For additional architectural details, refer to [12]. During inference, we adopt the DDIM method [46] with 100 denoising steps. The model is trained using the Adam optimizer [27] with a learning rate of 10^{-4} . The weight decay is set to 0. All experiments are performed on a single NVIDIA A100 GPU.

D. Encoder vs. Physical Buffer?

Many previous studies have used encoder-based methods to extract latent facial feature information from reference photos [51]. To evaluate whether the encoder can effectively extract enough facial features to guide the diffusion model in solving the low-light enhancement and denoising task, we conducted an experiment. As illustrated in Fig. 10, we utilized an encoder (ResNet-18 [19]) to extract latent codes from the target individual’s gallery photos. Following the method employed by ADM [12] for time embedding, we scaled and shifted the features in each layer of the diffusion model using the latent codes. This process integrates the identity information extracted by the encoder into the diffusion model.

We compared the restored images generated with the encoder-based method with the proposed physical buffer-guided method on our real-captured photo set. This is a special semi-real set, in which we take photos of some printed paper photos at night. We prepare this semi-real set because the ground-truth will be available to be compared with. The quantitative and visual comparisons are presented in Table 6 and Fig. 11, respectively. The results demonstrate that guiding the diffusion model using ID physical buffers produces significantly better identity preservation than the encoder-based approach. One major reason for this is that the ID physical buffers serve as robust conditions, enabling the extraction of comprehensive facial features from the gallery. In contrast, the encoder-based method is less focused on facial features and is often influenced by irrelevant factors such as background and hairstyle. Consequently, the latent codes extracted by the encoder are less effective in guiding the diffusion model to the personalized generative space compared to the ID physical buffers.

E. Gallery Photos

Fig. 13 presents the the gallery photos for the test subjects included in the Fig. 6 of the main paper.

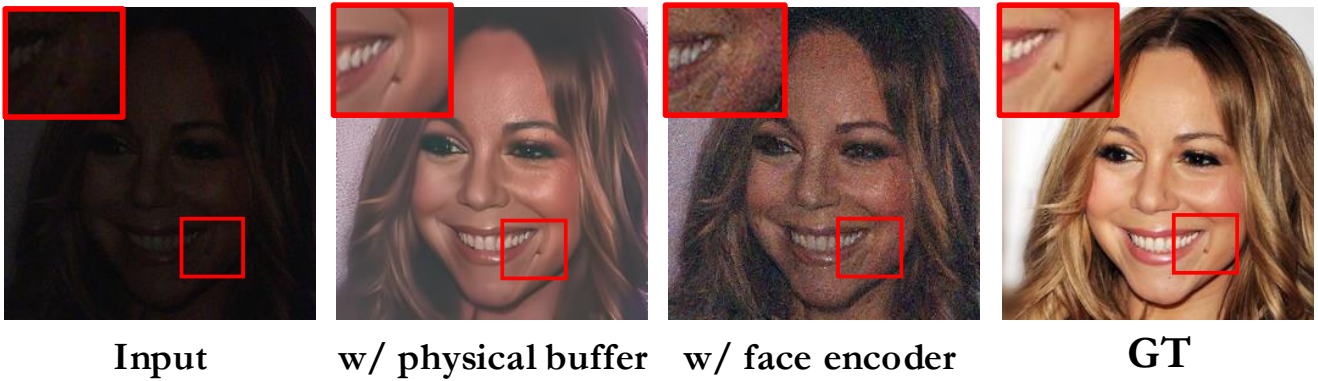


Figure 11. Visual comparison on different identity representation strategies (physical buffer and face encoder).

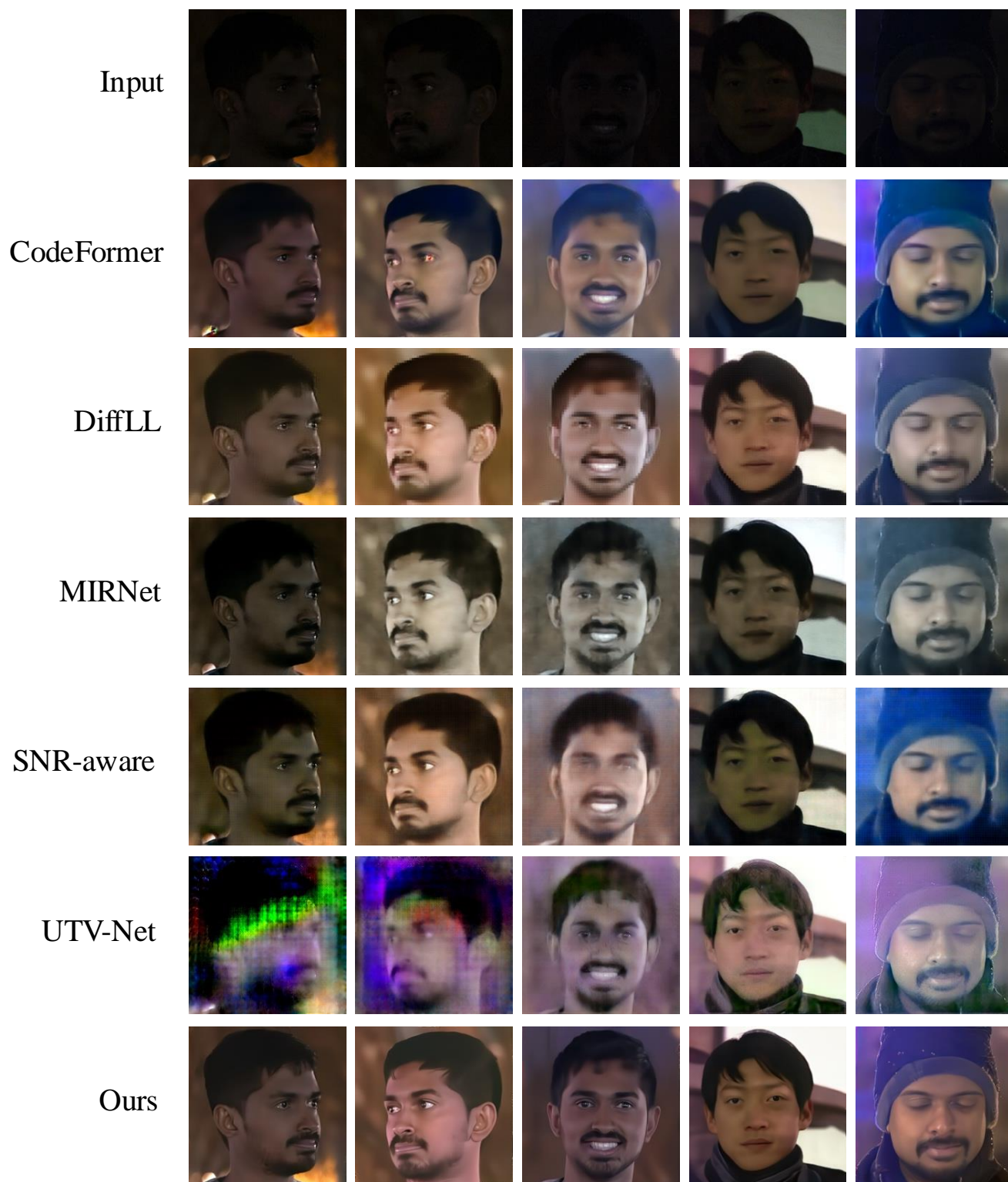


Figure 12. Additional real-captured visual comparison.

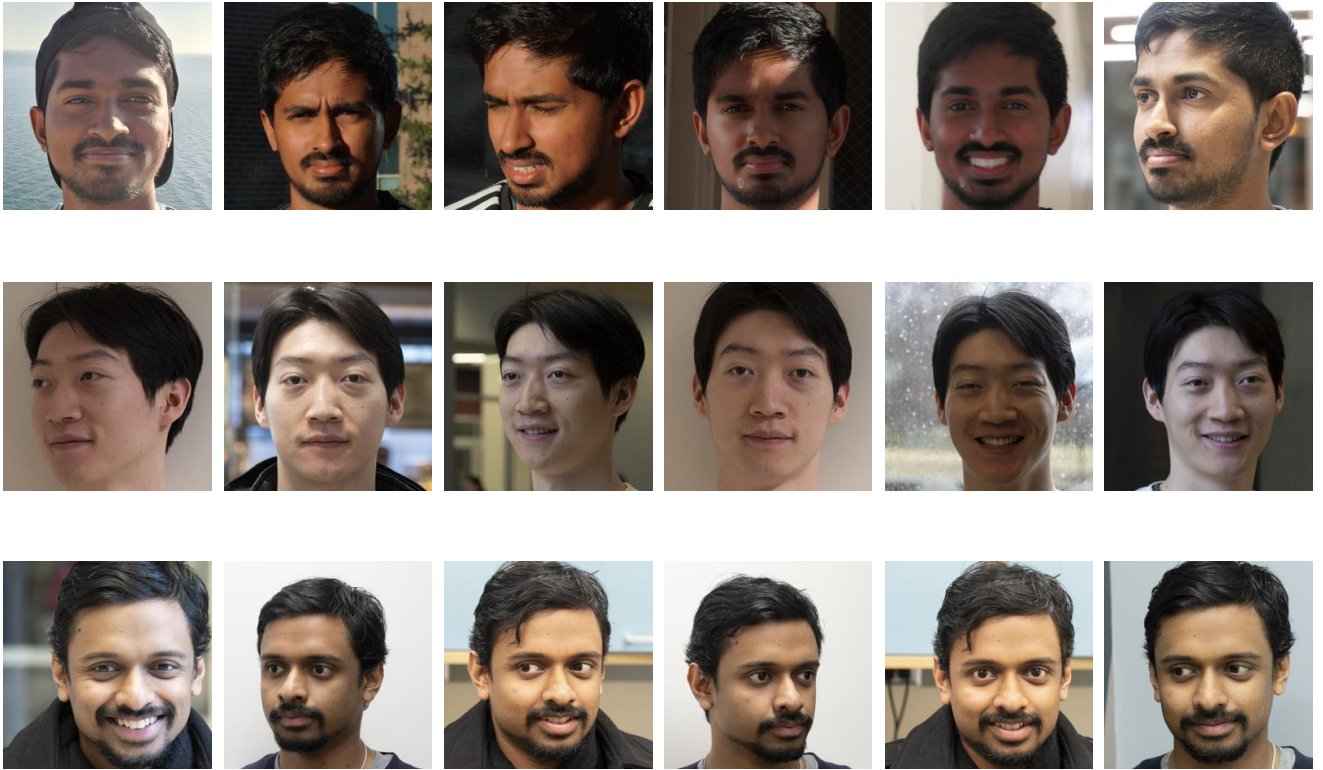


Figure 13. Gallery photos.



Figure 14. Additional visual comparison.

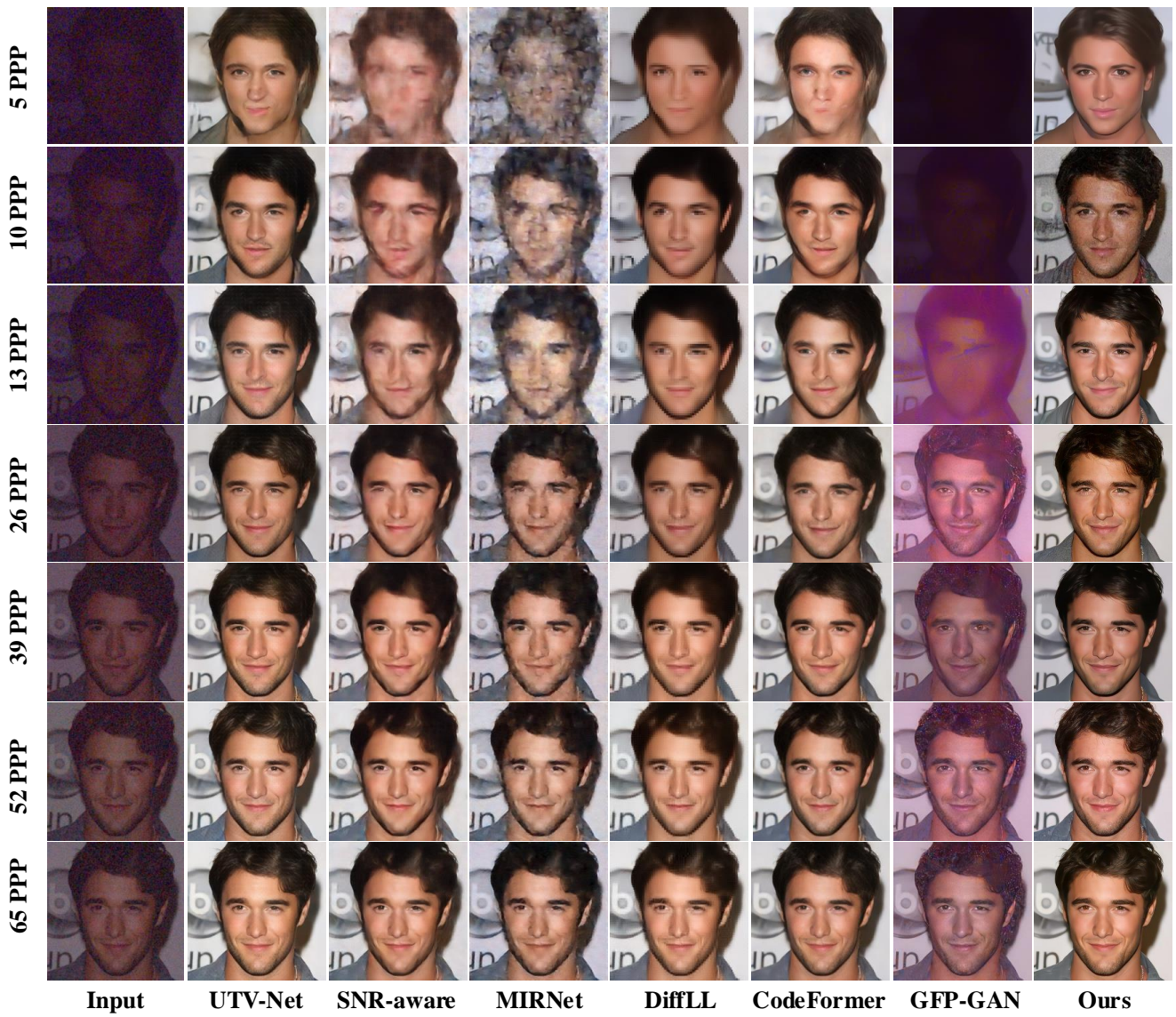


Figure 15. Additional visual comparison.